Study on the Melt Fracture of Metallocene Poly(Ethylene-Octene) in Capillary Flow

Zhenghong Tao, Jan-Chan Huang

Department of Plastics Engineering, University of Massachusetts Lowell, Lowell, MA 01854

Received 4 July 2004; accepted 28 December 2004
DOI 10.1002/app.22198
Published online in Wiley InterScience (www.interscience.wiley.com).

ABSTRACT: Shear viscosity and melt fracture of a metallocene poly(ethylene-octene) were studied using a capillary rheometer and dies with different lengths. The true wall shear stresses determined at zero die length showed a dip at high shear rates. The shear viscosity was derived from the true wall shear stress. With increasing shear rates, the extrudate staged from smooth to three types of melt fracture with regular patterns, and then turned into irregular shapes. Three types of regular melt fractures—sharkskin, helix, and spiral (in sequence)—were observed with an increase of the shear rates. The wavelength of the regular melt fracture was measured from extrudates, and the corresponding frequency was calculated. The frequency increased at elevated melt temperatures. Both shear viscosity and frequency at different temperatures correlated well by using the time–temperature Williams–Landel–Ferry (WLF) superposition. Additionally, it was found that the frequency decreased slightly for a longer die but it increased when the shear rate went up. Three frequency functions were associated with three melt fracture patterns, respectively. © 2005 Wiley Periodicals, Inc. J Appl Polym Sci 98: 903–911, 2005

Key words: melt fracture; melt viscosity; metallocene poly(ethylene-octene)

INTRODUCTION

Melt fracture is a flow instability phenomenon occurring when polymer melts are extruded through a die at rates exceeding a critical shear stress. Most of the previous studies on the melt fracture of polymers focused on the behavior of various types of polyethylenes (HDPE, LDPE, and LLDPE).[1–27] Melt fracture has been classified into two types. At a low shear rate, the extrudate develops a small-amplitude high-frequency disturbance on its surface, which is called sharkskin or surface melt fracture (SMF). Sharkskin generally occurs for polymers with a narrow molecular weight distribution. When the shear rate goes up, the second type of melt fracture is observed. It shows different behaviors depending on the type of flow. For a speed-controlled flow, a pressure oscillation is observed and large amplitude quasiperiodic patterns are developed. The flow is sometimes called a spurt flow. Both sharkskin and spurt flow are referred to as regular melt fractures in this article. When the shear rate keeps increasing, the flow sometimes becomes steady again and is followed by a second region of spurt flow with different melt fracture patterns. At even higher shear rate, gross melt fracture (GMF) eventually occurs. When a pressure-controlled flow is employed, a flow hysteresis curve occurs in some ranges of shear stresses where two different flow rates are associated with a single shear stress. It is indicated by a discontinuity in the plot of flow rate versus pressure drop.

Many studies have been devoted to sharkskin and spurt phenomena of PE. Two types of theories have been proposed for the mechanism of sharkskin. One is based on stick-slip at the die wall,[2,3,13–15] and the other is based on the periodic growth and relaxation of tensile stress[17–26] or the tearing and rupture[16,22,28,29] on the extrudate surface at the die exit. The spurt phenomenon has been interpreted by either the stick-slip phenomenon near the capillary surface,[1–6,23,24] compressibility of polymer melts,[7] combination of compressibility and slip,[8,9] or constitutive instability of polymer melts.[10–12] High density polyethylene (HDPE) with a high molecular weight tends to be free of sharkskin and enters directly into the spurt stage when shear rate increases. For linear low density polyethylene (LLDPE) with a narrow molecular weight distribution, sharkskin is frequently encountered preceding the spurt. Polymers produced by metallocene technology generally exhibit a molecular structure with a narrow molecular weight distribution. This makes metallocene polymers susceptible to melt fracture. The narrow molecular weight distribution also makes the metallocene polymer difficult to process. Polymer processability, which is represented by the melt flow index (MFI) ratio measured at 10 Kg and 2 Kg, I_{10}/I_2, can be improved through the incorporation of long chain branching (LCB).

Most studies on melt fracture emphasize the critical shear stress at the inception of melt fracture. The observation of the period or frequency of melt fracture is

Correspondence to: J.-C. Huang (Jan_Huang@uml.edu).

rarely reported. Recently, Wang and coworkers[23,24] measured the critical shear stress for a liner HDPE under controlled pressure and found that the onset stress for slip at different temperatures could be superimposed by using the WLF (Williams–Landel–Ferry) method. In later articles, Wang and coworkers[25,26] reported that the wavelength of sharkskin of LLDPE at different temperatures could also be superimposed by the WLF method. Furthermore, the period of melt fracture was found to be the same order of magnitude as the characteristic relaxation time measured by the oscillation shear flow. In our previous study[30] on Atofina 3181, a high molecular weight polypropylene (PP) with 0.75 MFI, we reported that the wavelength of extrudates in the regular melt fracture region increased when the shear rate was increased. However, the frequency of regular melt fracture was almost constant with increasing shear rates and it decreased slightly for a longer die. We also observed[31] that the frequency of melt fracture of PP with different molecular weights and at different temperatures could be superimposed using the shift factors obtained from viscosity data. The frequency was a function of shear rate and showed a small maximum around shear rate 1000 s^{-1}.

Additionally, the period or frequency can be used for interpretation of the mechanism of melt fracture. As discussed above, the melt fracture of PE usually involves both sharkskin and spurt flows. In the spurt stage the extrudate sometimes shows repeated bamboo-like and helix patterns. These spurt flows were interpreted by the stick-slip flow mechanism at the capillary wall. In a recent study by Kim and Dealy,[27] carbon black tracer was used to observe the melt fracture of HDPE. They reported pictures showing that the transition from SMF to GMF was accompanied by the rupture of carbon tracer at the center of the extrudate. From pictures of the extrudate surface, the transition was a gradual process and the extrudate remained quasi-periodic. It is therefore interesting to have a further study on the frequency of regular melt fracture at different stages of flow. A change in frequency probably indicates a different melt fracture mechanism. The purpose of this article is to continue the study on the frequency of melt fracture by using a metallocene poly(ethylene-octene), which also shows several melt fracture patterns.

EXPERIMENTAL

The resin used in this study was a commercial poly(ethylene-octene), Engage 8100, obtained from Dow Chemical Company. It was produced by INSITE metallocene technology and contained 38 wt % of 1-octene comonomer. The melt flow index was 1 g/10 min, and the Dow rheological index (DRI) was 2, as reported by the manufacturer. DRI is a measure of LCB. A higher DRI indicates a higher LCB. Guimaraes and coworkers[32] reported Mw = 323,000 for this polymer. A Galaxy V capillary rheometer (Kayness Inc., Model 8025) and tungsten carbide capillary dies with flat entrance region were used. All the tests were run at controlled speeds. The diameter of the orifice was 0.10 cm, and the lengths of the dies were 0.50, 2.0, and 3.0 cm, respectively. These gave die length-to-radius (L/R) ratios of 10, 40, and 60, respectively. Shear rates spanned from 10 to 5000 s^{-1}. Temperatures of 150, 190, and 230°C were chosen for this study. The extrudates coming out of the die were quenched immediately in a cold liquid to prevent relaxation. The wavelength of the extrudates was measured under an optical microscopy.

RESULTS AND DISCUSSION

General observation of melt fracture

The melt fracture of the polymer was observed from the extrudates. When melt fracture started, the extrudate did not maintain the smooth cylindrical geometry. Figure 1a illustrates the microscopic pictures of the extrudates from the longest die at the melt temperature of 150°C varying in the apparent shear rate. The melt fracture became visible under optical microscopy when apparent shear rates exceeded 50 s^{-1}. Three distinct patterns of the regular melt fractures were observed in sequence with increasing shear rate. At a melt temperature of 150°C, the extrudate surface started to have a fishnet pattern at shear rate as low as 50 s^{-1}. The fishnet-like pattern was formed by overlapped right-hand and left-hand helices in the same area. The depth of the groove resembled a surface melt fracture, and the stress level was 0.1–0.2 MPa. Since the stress level is related to the occurrence of sharkskin for other types of PE, this stage was identified as sharkskin.

Between 100 and 200 s^{-1}, the extrudate showed a helix with a regular pitch. The grove became deeper with an increase of the shear rate. Migler and colleagues[33] reported a similar melt fracture picture for a commercial metallocene poly(ethylene-octene) with lower content of octene. Once the shear rate exceeded 300 s^{-1}, a spiral pattern of the melt fracture developed gradually. The variation in extrudate diameter in this stage is higher than that in the previous helix stage. Above 800 s^{-1}, the regular pattern disappeared gradually and the extrudate came out with an irregular pattern, which could be referred to as the GMF stage. All these patterns of the melt fractures were also observed at elevated temperatures. However, the transition shear rates for each pattern moved to higher shear rates. As shown in Figure 1b, at the melt temperature of 230°C, the sharkskin extended from 100 to 300 s^{-1} and the helix pattern ended at 1000 s^{-1}. It was noted that the handedness of the rotation of the helix could turn in different directions at some shear rates, and

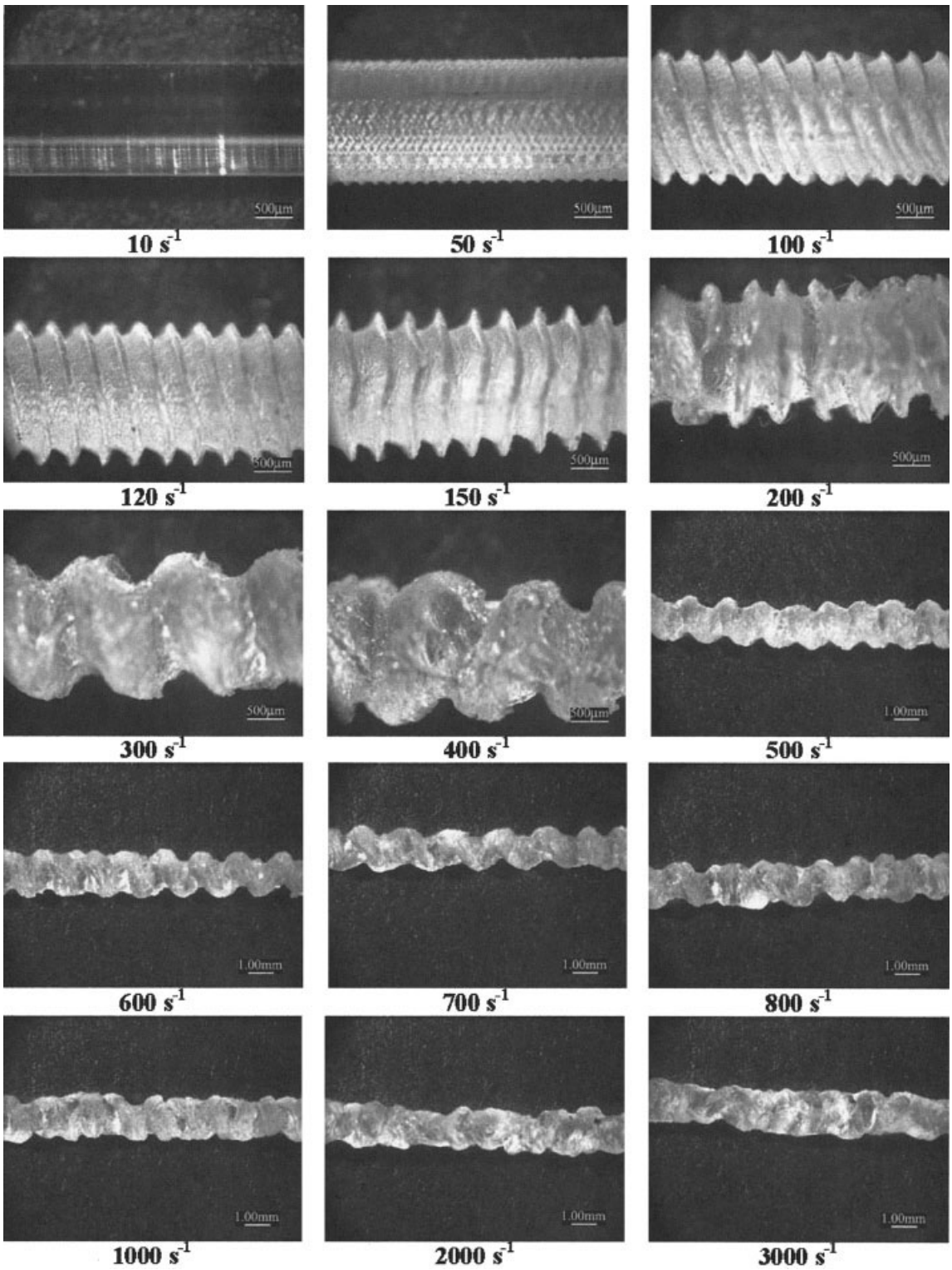

Figure 1 Extrudates of Engage 8100 using die with L/R = 60. (a) 150°C. Below 400 s^{-1} the ruler is 500 μm; above 500 s^{-1} the ruler is 1 mm. (b) 230°C. Below 1000 s^{-1} the ruler is 500 μm; above 2000 s^{-1} the ruler is 1 mm.

sometimes different orientations existed at different sides of the extrudate. But the difference from sharkskin was that there was only one type of groove in a location. The irregular pattern started around 2000 s^{-1}.

Figure 2 plots the apparent shear stress, $\tau_a = R\Delta P/2L$, versus the apparent shear rate, $\dot{\gamma}_a = 4Q/\pi R^3$ (Q is volume flow rate), for Engage at three temperatures with the longest die. The region for each pattern of melt fracture is delineated. It can be seen that both

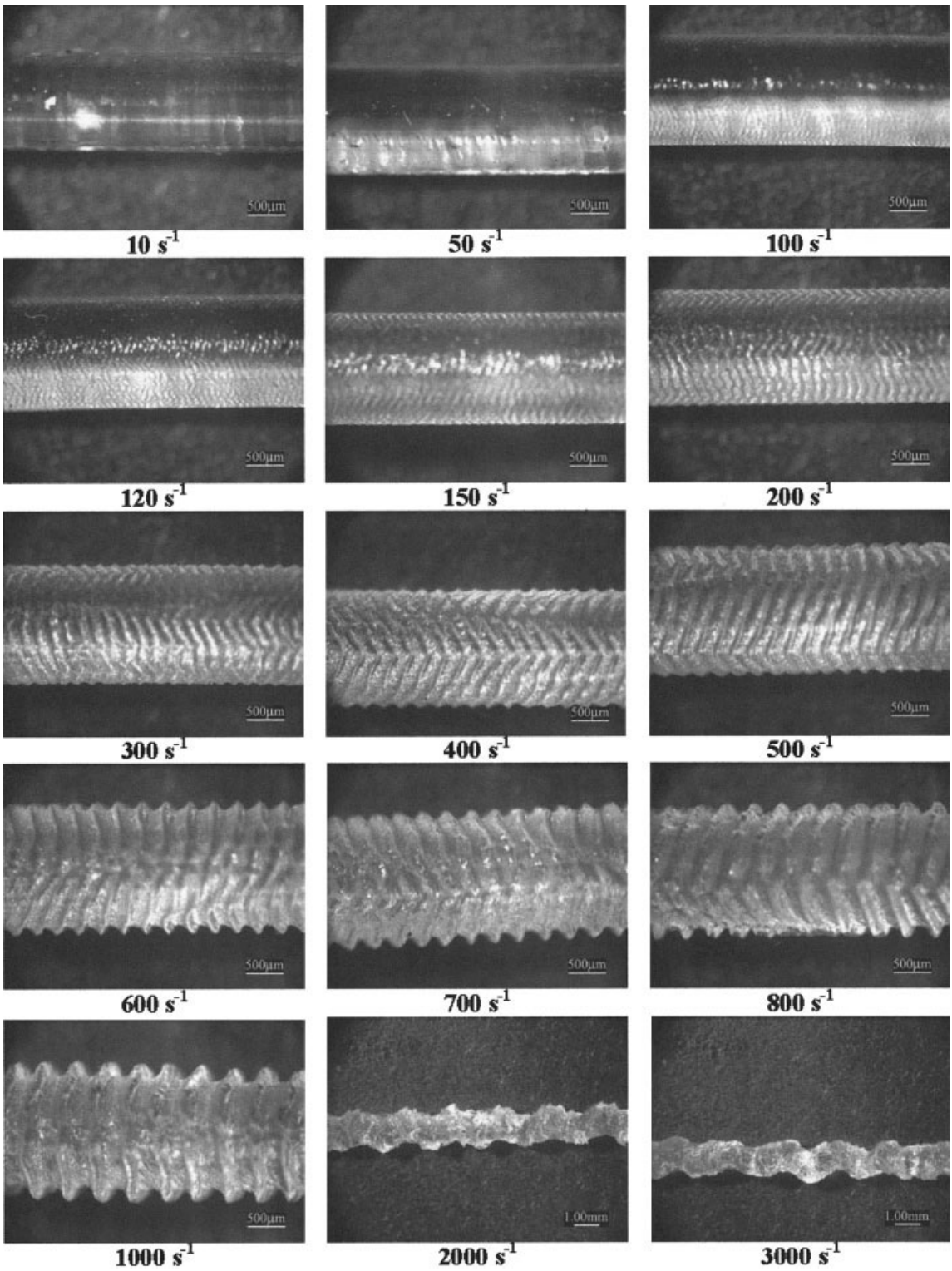

Figure 1 (*Continued from the previous page*)

sharkskin-helix and helix-spiral transitions occurred at constant shear stresses, respectively, at the three temperatures. But transitions from smooth to sharkskin and from spiral to GMF were less certain, due to the wider shear rate interval. The range for sharkskin widened when temperature increased, while the range for spiral narrowed down somewhat. Hatzikiriakos and colleagues[34] studied capillary flow of metallocene polyethylene (mPE) at 150°C and observed sharkskin only at a transition stage. This observation agrees with our result because at a low temperature, the range of sharkskin became very narrow. Kim and coworkers[35]

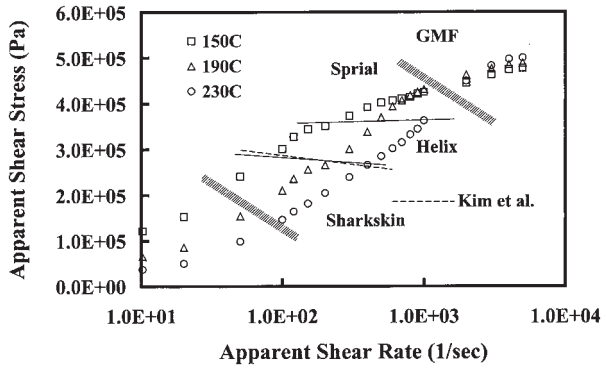

Figure 2 Apparent shear stress versus apparent shear rate of Engage 8100 at three temperatures for the die with L/R = 60. Lines and hatched area were drawn to delineate different melt fracture stages.

studied several commercial mPEs and reported melt fracture transitions at several temperatures. Their sample F1 agreed with the properties of Engage 8100. The onset of the melt fracture of this sample is indicated in Figure 2 and agrees very well with the sharkskin-helix transition in our study. They also reported that an increase of LCB would increase the onset shear rate of melt fracture. Similarly, Kim and Dealy[27] also reported the onset stress of melt fracture of mPE increased when LCB and polydispersity increased.

Pressure-die length relations

Figure 3 shows a plot of pressure-length relation for the three dies at 190°C. This plot is commonly used to identify the existence of melt fracture and wall slip.[1–4] For PE, polybutadiene, and polyisoprene, the melt fracture is commonly accompanied by a discontinuity in the shear stress versus shear rate curve,[5] while for PP no such discontinuity has been reported. In our study there was no discontinuity found for Engage. Recent work of Hatzikiriakos and coworkers[34] also reported no flow discontinuity in constant flow extrusion for mPE with LCB. Migler and colleagues[29,33] used an optical method to study the capillary flow of mPE and found that there was no slip on the wall; but when a fluoropolymer was added as the lubricant, slip on the wall was observed. In Figure 3 the apparent shear stresses were very close for the three dies, but a divergence of data started at apparent shear rates above 100 s^{-1}. The divergence coincided with the beginning stage of sharkskin. Above this shear rate, the extrudate had melt fracture with a regular pattern. At even higher shear rate, the melt fracture turned into an irregular shape.

The apparent shear stress increased with the apparent shear rate, as shown in Figure 3. But the slope at the high shear rate region turned gently, compared to the low shear rate region. This is typical for a material exhibiting a shear thinning phenomenon. The curves of the two longer dies overlapped each other and had lower shear stress than the shortest die in the high shear rate region. If there was no pressure effect on viscosity, the plot of pressure drop versus die length should be a straight line. This is the well-known Bagley plot.[36] When pressure drop of each flow rate was plotted against L/R, an upward trend was observed, the same as we found in our previous studies of PP.[30,31] This phenomenon can be explained by the pressure dependence of shear and extensional viscosities. Thus, the following function has been used to describe the effect of pressure on shear viscosity[36–40]:

$$\eta = \eta_o e^{\beta P} \tag{1}$$

where η_o is the shear viscosity at zero pressure and β is the pressure coefficient. A similar expression has also been used to describe pressure dependency on extensional viscosity.[41,42] In our previous work,[30,31] we derived an analytical equation to describe the relationship between the pressure drop and die length, and the pressure coefficients reported by Bindings and colleagues[41] were used to calculate the true wall shear stress and end effect at zero pressure. From this information, shear viscosity and extensional viscosity at zero pressure were calculated. However, because the pressure coefficients of shear and extensional viscosity of Engage were not available, a different method was used in this study. A second order polynomial was used to fit pressure versus die length data, and the slope at zero die length was calculated as the true wall shear stress. This is shown in Figure 4 for selected conditions. The second order polynomial was sufficient because the curve was only slightly nonlinear.

Shear viscosity

For most unfilled polymers the rheological properties at different temperatures can be superimposed into a master curve using a reference temperature. A data

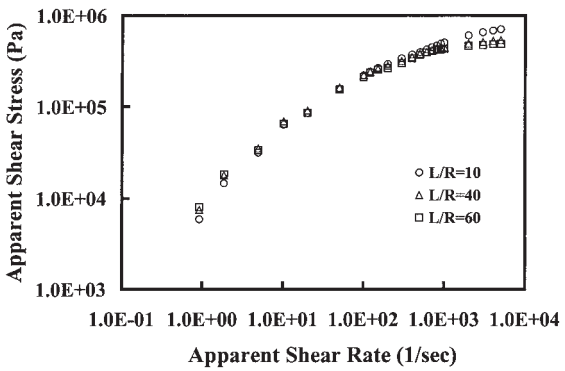

Figure 3 Apparent shear stress versus apparent shear rate of Engage 8100 at 190°C for three die lengths.

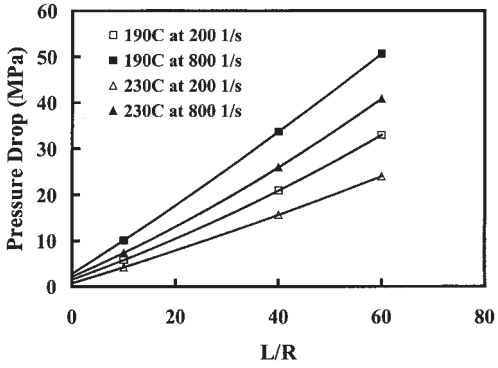

Figure 4 Pressure drop versus L/R of Engage 8100 at 190°C and 230°C for apparent shear rate at 200 and 800 s^{-1}.

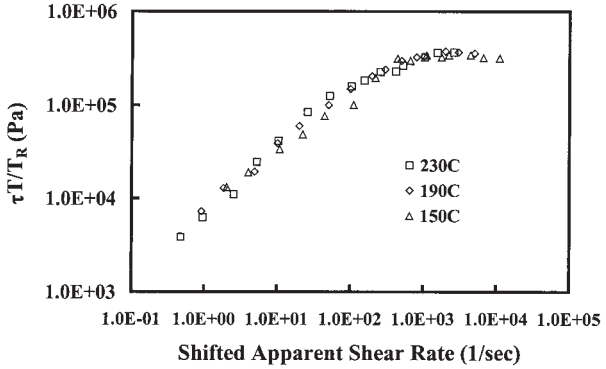

Figure 5 True wall shear stress, $\tau(T)T_R/T_o$,, versus shifted apparent shear rate ($a_T\ \dot{\gamma}_a$) at 190°C.

superposition can be made for wall shear stress versus shear rates based on the following formula:[43]

$$\tau(T)T_R/T = f(a_T\dot{\gamma}) \tag{2}$$

where a_T is the WFL shift factor and T_R is the reference temperature, which was 190°C in this study. The results are listed in Table I. For the same polymer measured at different temperatures, the shift factor was related to flow activation temperature of melts. The activation energy of shear viscosity was estimated to be 32 kJ/mol, which agreed with the result of Kim and coworkers.[35] The activation energy of PE is known to increase when LCB increases.[35,44,45] At zero LCB the value is about 21 KJ/mol, while for high LCB the value could reach 36 KJ/mol. Our activation energy indicated the LCB density of Engage exceeded 0.5 per 10,000 carbons. The superposition of the shear stress curve is shown in Figure 5. It can be seen that at high shear rate, the shear stress started to decrease. Hatzikiriakos and colleagues[34] reported a decrease in the slope at shear stress of about 0.3 MPa, and the plot reached a plateau at shear rate around 1000 s^{-1}. These features are consistent with this study. From the Doi–Edwards theory[46] and its modifications,[10–12] a maximum in the stress versus shear rate curve produces instability and creates a constitutive instability of a flow, resulting in melt fracture. The shear rate of the plateau region corresponded to the spiral-GMF transition of this study.

The calculation of shear viscosity started from a plot of the true wall shear stress, $\tau_{tw,}$ versus the apparent shear rate, $\dot{\gamma}_a$, on a double logarithm scale. The slope n of this plot was used to make the Rabinowitsch correction. The Rabinowitsch correction was made to calculate the true shear rate on the capillary surface, $\dot{\gamma}_{tw}$, from the apparent shear rate, $\dot{\gamma}_a$:

$$\dot{\gamma}_{tw} = \dot{\gamma}_a(3n + 1)/4n \tag{3}$$

The shear viscosity was calculated as:

$$\eta = \tau_{tw}/\dot{\gamma}_{tw} \tag{4}$$

The melt viscosity results of polymers at different temperatures can also be superimposed with proper adjustment of parameters. A superposition of data can be made for the shear viscosity based on the following formula:[43]

$$\eta(T)T_R/a_TT = f(a_T\dot{\gamma}) \tag{5}$$

The same shift factors in Table I were used. Equation (5) predicts a master curve for shear viscosity, which is shown in Figure 6. It can be seen that the shear viscosities of Engage at three temperatures overlapped well after the shifts. The results of the shear viscosity

TABLE I
The Shift Factor of EG 8100 at Different Temperatures

Materials	Shift factor, a_T
150°C	2.2
190°C	1.00
230°C	0.52

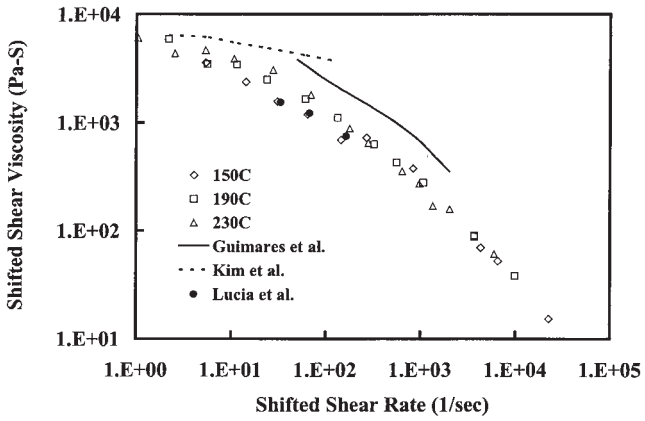

Figure 6 Shifted shear viscosity, $\eta(T)T_R/a_TT_o$, versus shifted shear rate ($a_T\ \dot{\gamma}_a$) at 190°C.

in Figure 6 also demonstrated a strong shear rate dependency in the shear rate region, which justified the use of the Rabinowitsch correction. Despite the occurrence of melt fracture, the viscosity results showed a continuous trend and could be superimposed. This suggested that the pressure drop associated with the melt fracture was separated from the wall shear stress in the plot of Figure 4 and was likely to be associated with the entrance effect or was created at the die exit similarly to other PEs.[16–24, 47] The results of Engage 8100 at 190°C by Guimaraes and coworkers[32] were compared in Figure 6. Also compared are the results of Kim and colleagues[35] and Lucia and coworkers.[48] The former group presented their results for shear rate below sharkskin, and the latter group reported the results for 220°C. After shifting to 190°C by using the shift factor of this study, the results agreed with ours. As illustrated in Figure 6, the results of Kim and colleagues and Guimaraes and coworkers were slightly higher than ours. This may have been because they did not use the Bagley correction; without the separation of the entrance pressure drop, the wall shear stress and shear viscosity would be higher. Another possibility may have been the pressure effect, which also increased the viscosity. In this study, wall shear stress was calculated from the slope at zero die length, which is normally smaller than the apparent shear stress.

Frequency of melt fracture

For LLDPE, sharkskin usually occurs before spurt flow.[1–8] From Figure 1 we found that sharkskin also occurred in Engage. Above another critical stress, the melt fracture showed large amplitude periodic patterns. The wavelength increased when shear rate was increased. Since the observed wavelength might change due to stretching the extrudate, it was better to express the oscillation using frequency at the die exit condition. The ratio between the average melt flow velocity and the wavelength at the capillary exit represented the frequency of oscillation. The frequency was calculated using the following formula:[31]

$$v = \langle V \rangle / \lambda = \dot{\gamma}_a / D / 8 / \text{wavelength of solid extrudates} / (D_{ex}/D)^2 / (\rho_{25C}/\rho_T) \quad (6)$$

where <V> is the average velocity at the die exit, λ is the wavelength measured at the die exit condition, D_{ex} is the average diameter of the solid extrudate, and D is the diameter of the die. In eq. (6) the measured wavelength of extrudates was adjusted by die swell and density ratio, ρ_{25C}/ρ_T, to reflect the actual wavelength at the die exit. Density of Engage melt at different temperature was measured according to ASTM 3855–02. A similar equation was used by Wang and colleagues[26] in the calculation of wavelengths of melt fracture in the sharkskin stage of LLDPE. The use of frequency avoids gravitational sagging, which might lead to increasing the wavelength and reducing the extrudate diameter at the same time. The effects of both were cancelled out in the calculation.

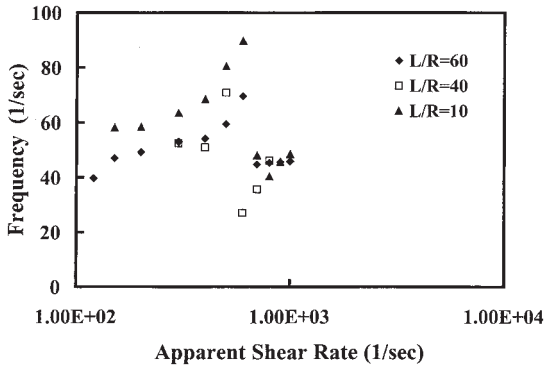

Figure 7 Frequency of regular melt fracture versus apparent shear rate of Engage 8100 at 190°C for three dies.

Figure 7 shows the frequency of regular melt fracture versus the apparent shear rate for the three dies at 190°C. The frequency was smaller for the longer dies. A discontinuity was observed at shear rate 800 s^{-1}. Below this shear rate, the extrudate showed a helix pattern and above that a spiral pattern. The critical shear rate for the transition was not affected by the die length. The pressure oscillation of some PEs was reported to be dependent on barrel size.[3,9,49] In this study, the flow properties from high shear rates to low rates did not show any significant difference from the results obtained by extruding from low rates to high rates. It could be concluded that the frequency in our study was independent of the barrel size.

In a previous study,[31] we proposed to use the WLF shift to bring the frequency of PP with different molecular weights and temperatures into master curves. Different frequency may be attributed to change in melt viscosity or relaxation time associated with viscosity. If melt fracture frequency is related to melt viscosity, it can be shifted; and the results from different samples can be superimposed together. Since both shear rate and frequency have the same dimension, 1/time, they will be shifted by the same factor. In Figure 8 both frequency and shear rate of the longest die were adjusted by the shift factors in Table I to form three master curves. For 150°C the lowest shear rate was a sharkskin pattern. At higher shear rates, the melt fracture changed into a helix and the frequency decreased. The helix curve extended the rapidly increasing trend until another transition at $\dot{\gamma}$ = 800 s^{-1}. The results are summarized in three curves, which all increased with increasing shear rate. The range of frequency was between 40–80 s^{-1}, which was between the sharkskin of LLDPE at 200°C[25,26] and the spurt of PP at 190°C.[30]

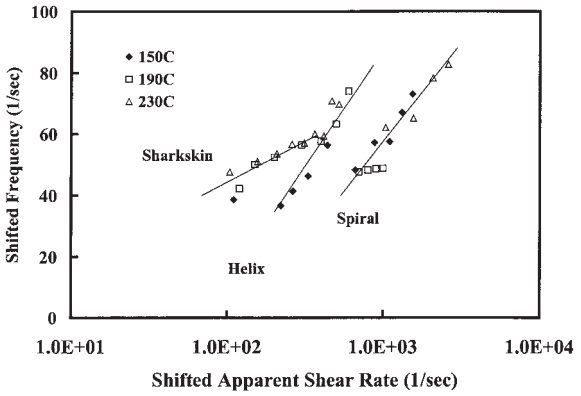

Figure 8 Shifted frequency ($a_{T\nu}$) versus shifted apparent shear rate ($a_T\ \dot{\gamma}_a$) of Engage 8100 for the die with L/R = 60. Lines were drawn to show the trend.

The mechanism commonly used to explain the spurt of PE is the slip-stick phenomenon combined with the compressibility of melts.[1–6] In this mechanism,[50] a high strain is first built up in the melt in the area near the die surface, where shear stress is the highest. The polymer molecules are stretched in the flow direction, and a slip occurs after the stress exceeds a threshold value. During this stage, a change in pressure or flow rate can be observed. After slipping, the molecules are relaxed. The cycle repeats, leading to the periodic pattern. The melt fracture of Engage may involve similar processes. The fact that frequency could be superimposed was supportive evidence showing the involvement of an interchain strain relaxation process in such spurt phenomena of Engage. Our observation on the decrease of frequency with increasing die length could also be explained by this mechanism because the strain would be higher in a shorter die where strain was just starting to relax from the die inlet. Another reasonable explanation is that a longer die had a higher hydrostatic pressure, which led to higher viscosity, slower relaxation process, and smaller melt fracture frequency. The increasing trend observed in Figure 8, when frequency increased, could also be explained within a similar framework.

Recently, Wang and colleagues[26] employed the Maxwell model to give an interpretation of the mechanism for sharkskin. In the model the stress at the wall was repeating a stress buildup and decay process. During the decay process the following equation can be derived:

$$\sigma(t) = \sigma_s + (\sigma_c - \sigma_s)\ \mathrm{Exp}\ (-t/\tau'), \qquad \text{for } 0 \le t < \tau_R \tag{7}$$

where σ_s is the stress corresponding to the shear rate at slip at the wall, σ_c is the wall shear stress without slip, and τ' is the relaxation time of the Maxwell model. At the end of the relaxation period, $t = \tau_R$ and the stress relaxed to $\sigma(\tau_R) = \sigma_h$. During the stress buildup process, the following equation applied:

$$\sigma(t) = \sigma_h + \sigma_c\{1 - \mathrm{Exp}\ [-(t - \tau_R)/\tau']\}, \qquad \text{for } \tau_R \le t < \tau_R + \tau_G \tag{8}$$

The overall oscillation period is given by:

$$\tau = \tau_R + \tau_G = \tau'\ \ln\left[\frac{R^2(S-1)}{(S-R)}\right] \tag{9}$$

where $R = \sigma_c/\sigma_h$ and $S = \sigma_c/\sigma_s$. The overall oscillation period is related to the time constant of the Maxwell model by a logarithmic factor. The value of R represents the ratio of the upper bound, σ_c, and the lower bound, σ_h, of stress during the oscillation. The values of σ_h and σ_c increase when the extrusion rate increases, but their ratio R likely remains constant at a value slightly higher than unity.[51] Ratio S represents the ratio between the nominal (no slip) stress to the threshold stress, σ_s. The value of S is higher than R and increases when extrusion rate increases. If R remains constant while S increases, the value of the log term will decrease continuously. This could explain a decrease of oscillation period and the increase of frequency when the extrusion rate rises. The model also explains the proportional relation between the period of sharkskin and the characteristic time of the polymer, but cannot explain the transition to a different curve. The transition of the functions in Figure 8 was likely associated with different instability mechanisms, which resulted in different melt fracture patterns. In the model of Doi and Edwards,[46] a dip of τ versus $\dot{\gamma}$ leads to melt fracture. In our study the peak in Figure 3 occurred at $\dot{\gamma} = 1000\ s^{-1}$, which corresponded to the spiral-GMF transition. The two earlier transitions probably related to the relaxation process on the capillary surface or rupture of the extrudate surface. Since frequency at the three regular melt fractures could be superimposed, these melt fractures likely belonged to a cohesive failure mechanism,[33] or occurred between bulk chains and adsorbed chains,[25,26] rather than between polymer and capillary wall. A further study on frequency using different capillary surface might offer more insight.

The frequency in Figure 8 was in the range of 40–80 s^{-1}. In our previous study using PP with Mw = 512,000 at 190°C, the range was 2–4 s^{-1}. The frequency of HDPE reported by Wang and colleagues was in the range of 50–200 s^{-1}. The difference between frequencies of different materials could be explained by the difference in the molecular weight and relaxation time. According to Lin,[11] the longest reptational relaxation time, τ_c, was related to Mw and the entanglement molecular weight, M_e, by the following formula:

$$\tau_c = K\frac{Mw^3}{Me}[1 - \sqrt{Me/Mw}]^2 \qquad (10)$$

where K is a constant proportional to the frictional coefficient of the polymer chain. The equation indicates τ_c increases when Mw increases. This leads to a decrease in frequency, which was demonstrated in PP.[31] The τ_c is also inverse to M_e, which depends on the nature of the monomer. The entanglement molecular weight of HDPE is about 1300[52] and for PP is about 7000.[53] An even higher M_e for polystyrene (35,000) and poly(dimethyl siloxane) (30,000) was used to explain the lack of sharkskin for these materials.[23] The entanglement molecular weight of mPE was not available to us, but could be estimated[54] by using the plateau of the loss modulus, G^o_N, in dynamic measurement using the relation: $G^o_N = \rho RT/M_e$. The values for mPE were in the range of 0.2 MPa.[32,43,54] This gave M_e about 15,000 g/mol. The high value of M_e for mPE could explain the small value of frequency, compared to HDPE.

CONCLUSIONS

Melt fracture properties of a poly(ethylene-octene) in capillary flow were studied. The flow curve and extrudate appearance could be divided into three regions. At low flow rate, smooth extrudate was obtained. With increasing flow rate, melt fracture with regular patterns occurred. At even higher shear rate, irregular melt fracture was observed. Shear viscosity was calculated and correlated well using WLF superposition. The frequencies of regular melt fracture were also superimposed by using the same shift factors obtained from shear viscosity. Three master curves were clearly related to the different melt fracture behaviors. Additionally, the frequency increased with increasing shear rate and was slightly higher for the short die. Based on the results of the frequencies of the melt fracture patterns, this study concluded that below the shear rate for GMF there were three regular melt fracture stages.

The authors would like to express their special appreciation to Dr. R. D. Deanin of the Department of Plastics Engineering at the University of Massachusetts Lowell for his invaluable help and useful discussion.

References

1. Sornberger, G.; Quantin, J. C.; Fajolle, R.; Vergnes, B.; Agasant, J. F. J Non-Newtonian Fluid Mech 1987, 23, 123.
2. Ramamurthy, A. V. J Rheol 1986, 30, 337.
3. Kalika, D. S.; Denn, M. M. J Rheol 1987, 31, 815.
4. Larson, R. G. Rheol Acta 1992, 31, 213.
5. (a) Denn, M. M. Annu Rev Fluid Mech 1990, 22, 13; (b) Denn, M. M. Annu Rev Fluid Mech 2001, 33, 265.
6. Shore, J. D.; Ronis, D.; Piche, L.; Grant, M. Phys Rev Lett 1996, 77, 655.
7. Weill, A. Rheol Acta 1980, 19, 623.
8. Hatzikiriakos, S. G. Polym Eng Sci 1994, 34, 1441.
9. Hatzikirakos, S. G.; Dealy, J. M. J Rheol 1992, 36, 845.
10. McLeish, T. C. B.; Ball, R. C. J Polym Sci Polym Phys Ed 1986, 24, 1735.
11. Lin, Y. H. J Rheol 1985, 29, 605.
12. McLeish, T. C. B. J Polym Sci 1986, B25, 2253.
13. Kissi, N. E.; Piau, J. M. J Non-Newtonian Fluid Mech 1990, 37, 55.
14. Hatzikiriakos, S. G.; Hong, P.; Ho, W.; Stewart, C. W. J Appl Polym Sci 1996, 55, 595.
15. Ghanta, V. G.; Riise, B. L.; Denn, M. M. J Rheol 1999, 43, 435.
16. Cogswell, F. N. J Non-Newtonian Fluid Mech 1977, 2, 37.
17. Piau, J. M.; Kissi, N. E.; Tremblay, B. J. J Non-Newtonian Fluid Mech 1990, 34, 145.
18. Moynihan, R. H.; Baird, D. G.; Ramanathan, R. J Non-Newtonian Fluid Mech 1990, 36, 255.
19. Tremblay, B. J. J Rheol 1991, 35, 985.
20. Kissi, N. E.; Piau, J. M. J Rheol 1994, 38, 1447.
21. Baird, D. G.; Tong, P. P. SPE Technical Paper, 53rd ANTEC 1995, 1095.
22. Kissi, N. E.; Piau, J. M.; Toussaint, F. J Non-Newtonian Fluid Mech 1997, 68, 271.
23. Wang, S. Q.; Drda, P. A. Macromolecules 1996, 29, 2627.
24. Wang, S. Q.; Drda, P. A. Macromolecules 1996, 29, 4115.
25. Wang, S. Q.; Drda, P. A.; Inn, Y. W. J Rheol 1996, 40, 875.
26. Barone, J. R.; Plucktaveesak, N.; Wang, S. Q. J Rheol 1998, 42, 813.
27. Kim, S.; Dealy, J. M. Polym Eng Sci 2002, 42, 482; (b) Kim, S.; Dealy, J. M. Polym Eng Sci 2002, 42, 495.
28. Inn, Y. W. R.; Fischer, R. J.; Shaw, M. T. Rheol Acta 1998, 37, 573.
29. Migler, K. B.; Son, Y.; Qiao, F.; Flynn, K. J Rheol 2002, 46, 383.
30. Huang, J. C.; Tao, Z. J Appl Polym Sci 2003, 87, 1587.
31. Tao, Z.; Huang, J. C. Polymer 2003, 44, 719.
32. Guimaraes, M. J. O. C.; Coutinho, F. M. B.; Rocha, M. C. G.; Farah, M.; Bretas, R. E. S. J Appl Polym Sci 2002, 86, 2240.
33. Migler, K. B.; Lavallee, C.; Dillon, M. P.; Woods, S. S.; Gettinger, C. L. J Rheol 2001, 45, 565.
34. Hatzikiriakos, S. G.; Kazatchkov, I. B.; Vlassopoulos, D. J Rheol 1997, 41, 1299.
35. Kim, Y. S.; Chung, C. I.; Lai, S. Y.; Hyun, K. S. SPE Technical Paper, 53rd ANTEC 1995, 1122.
36. Bagley, E. B. J Appl Phys 1957, 28, 624.
37. Kazatchkov, I. B.; Hatzikiriakos, S. G.; Stewart, C. W. Polym Eng Sci 1995, 35, 1864.
38. Huang, J. C.; Leong, K. S. J Appl Polym Sci 2002, 84, 1269.
39. Huang, J. C.; Shen, H. F. Adv Polym Tech 1989, 9, 211.
40. Denn, M. M. Polym Eng Sci 1981, 21, 65.
41. Binding, D. M.; Couch, M. A.; Walters, K. J Non-Newtonian Fluid Mech 1998, 79, 137.
42. Christensen, J. H.; Kjaer, E. M. SPE Technical Paper, 56th ANTEC 1998, 985.
43. Ferry, J. D. Viscoelastic Properties of Polymers; Wiley: New York, 1980; 3rd ed, Chapter 11.
44. Yan, D.; Wang, W. J.; Zhu, S. Polymer 1999, 40, 1737.
45. Vega, J. F.; Santamaria, A.; Munoz-Escalona, A.; Lafuente, P. Macromolecules 1998, 31, 3639.
46. Doi, E.; Edwards, S. F. The Theory of Polymer Dynamics; Clarendon Press: Oxford, 1986.
47. Piau, J. M.; Kissi, N. E., Tremblay B. J Non-Newtonian Fluid Mech 1988, 30, 197.
48. Silva, A. L. N.; Roche, M. C. G.; Coutinho, F. M. B.; Bretas, R; Scuracchio, C. J Appl Polym Sci 2000, 75, 692.
49. Becker, J.; Bengtsson, P.; Klason, C.; Kubat, J.; Saha, P. Int Polym Proc 1991, 6, 318.
50. Brochard, F.; de Gennes, P. G. Langmuir 1992, 8, 3033.
51. Okubo, S.; Hori, Y. J Rheol 1980, 24, 253.
52. Wood-Adams, P. M.; Dealy, J. M.; deGroot, A. W.; Redwine, O. D. Macromolecules 2000, 33, 7489.
53. Van Krevelen, D. W. Properties of Polymers; Elsevier Sci Pub Co; Amsterdam, 1976; Chapter 15.
54. Vega, J. F.; Muniz-Escalona, A.; Santamaria, A.; Munoz, M. E.; Lafuente, P. Macromolecules 1996, 29, 960.